

Silica-encapsulated magnetic nanoparticles formed by a combined arc evaporation/chemical vapor deposition technique

Kevin L. Klug, Vinayak P. Dravid,^{a)} and D. Lynn Johnson

Department of Materials Science and Engineering, Northwestern University, Evanston, Illinois 60208

(Received 6 November 2002; accepted 28 January 2003)

A multistep technique has been developed for the generation of metallic/alloy nanoparticles coated with amorphous silica. As a proof of concept, an inert-gas blown-arc geometry was used to create nanoparticles from a bulk nickel source, and silica coating formation was accomplished via tetraethyloxysilane (TEOS) decomposition over the nanoparticles in an adjacent chemical vapor deposition chamber. The composite particles exhibit resistance to hydrochloric acid attack over extended times, thereby confirming the protective nature of the silica coating, and magnetic measurements indicate a superparamagnetic transition temperature of 41 K. TEOS flow rate was found to have a profound effect on particle morphology, and individually coated dispersed particles were observed for the intermediate flow rate studied. These results, combined with the well-established field of silica functionalization, offer the possibility that a variety of industrially significant coated magnetic nanostructures may be synthesized with this versatile approach.

I. INTRODUCTION

Nanoparticles have received considerable attention in the past two decades due to the interesting properties afforded by their size. Their magnetic properties are of particular interest for the work at hand. Depending upon factors such as composition, average size, size distribution, and temperature, nanoparticles can exhibit magnetic behavior ranging from highly coercive to superparamagnetic. As a result of this wide spectrum of available coercivities, these materials may find use in such diverse applications as biomedical agents,^{1–4} ferrofluids,⁵ and magnetic data storage.^{6–8}

Despite their appeal, metallic nanoparticles are hampered by issues of chemical stability, dispersion, and surface functionalization. Due to their large surface area to volume ratio, such materials are susceptible to attack by oxidative or corrosive environments that can alter their chemistry and diminish their properties. One strategy that has been developed to overcome this obstacle is to generate a protective coating (e.g., graphite or silica) around the particles. Graphite coatings have been promoted

through the use of modified Kratschmer–Huffman arc evaporation geometries^{9–18} and hydrocarbon decomposition.¹⁹ However, it has proven difficult to synthesize separable, individually coated particles due to the encapsulating carbon's tendency to form crystalline networks around groups of particles. As revealed in this paper, amorphous silica offers an attractive alternative to the use of carbon coatings.

Chemical techniques have been used to form silica coatings on nanoparticles of various materials including nickel,²⁰ iron,^{21–23} iron oxide,^{24–26} a nickel/iron composite,²⁷ gold,^{28,29} silver,^{30,31} germanium,³² copper,³³ barium titanate,³⁴ and others. In addition to providing an adherent protective coating around the core particles, silica has the added advantage that it may be functionalized (e.g., Refs. 35–42) and thereby tailored for different applications. Selected examples of functionalization include techniques to couple single-phase silica particles with gold,^{43,44} DNA,⁴⁵ and fullerenes.⁴⁶ The functionalization of silica-coated magnetic nanoparticles offers an opportunity to expand the realm of tailored materials even further.

The direct chemical methods used to form the encapsulated nanoparticles listed above can result in impure products that require additional refinement. The high temperatures of such oxidative or reductive treatments not only complicate the synthesis process but may also result in particle growth.^{23,27} To circumvent these concerns, we have developed a hybrid physical/chemical

^{a)}Address all correspondence to this author.

e-mail: v-dravid@northwestern.edu

This author was an editor of this journal during the review and decision stage. For the *JMR* policy on review and publication of manuscripts authored by editors, please refer to <http://www.mrs.org/publications/jmr/policy.html>.

method to produce silica-encapsulated nanoparticle species. The nanoparticle cores were prepared by evaporating the desired pure metal in an electric arc, followed by silica coating formation via tetraethoxysilane (TEOS) decomposition in an adjacent chamber. By adjusting the amount of TEOS introduced during the procedure, it was possible to change the morphology of the coated magnetic powder, and individually coated particles were observed for the intermediate TEOS flow rate studied.

II. EXPERIMENTAL

The apparatus used to produce silica-coated magnetic nanoparticles was described elsewhere in detail^{19,47} and is shown schematically in Fig. 1. The basic system design includes four main components: an arc evaporation chamber; a chemical vapor deposition (CVD) furnace; a collection mechanism; a powder reservoir. Nanoparticles were formed in the first chamber by arc evaporation (100 A, approximately 25 V) of a 0.25-in.-diameter nickel rod (99.999% purity), followed by quenching of the metal vapor with a 25 m/s helium jet passing through the arc. The particle/inert gas aerosol was then forced into the CVD furnace, where the silica precursor vapor was introduced with an argon carrier gas that had passed through three consecutive liquid TEOS-containing quartz bubblers. On the basis of the equilibrium vapor pressure of TEOS at 20 °C (1 torr), the argon flow rate was adjusted to deliver 5, 2.5, 1.5, and 0.5 sccm of TEOS into the chamber, which was maintained at a pressure of 200 torr. The total helium flow rate (from the quench jet

and an additional inlet) was approximately 26 slpm. The reaction furnace's three heating zones were each set to 700 °C.

Following production, each of the four samples was subjected to ultrasonication in hydrochloric acid for several hours to remove any uncoated nickel in the products. Methanol and multiple centrifugation cycles were used to selectively remove the acid, and the remaining powder was dried under flowing nitrogen. This purification treatment ensured that the surviving powder consists of SiO_x-coated nickel particles that are well protected from aggressive environments.

A Hitachi HF 2000 cold field emission transmission electron microscope operated at 200 kV was used to determine the morphology of each acid-treated sample, and magnetic measurements were taken using a Quantum Design brand superconducting quantum interference device (SQUID) magnetometer.

III. RESULTS

A. Hydrochloric acid treatment

Table I displays the percentage of each sample that survived acid treatment, based on the as-collected and acid-treated dry powder masses. Note that this technique provides a useful qualitative comparison between the samples but does not discriminate between the relative amount of silica and coated nickel in the acid-treated product. The results in Table I reveal a direct correlation between the TEOS flow rate and the sample survival rate.

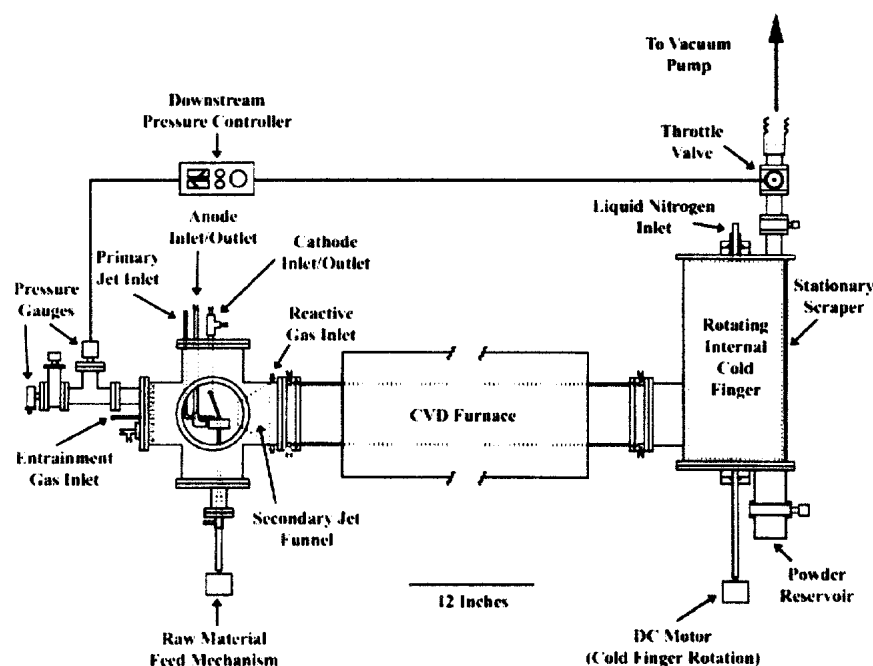


FIG. 1. Schematic of the nanoparticle synthesis apparatus.

B. Powder morphology

Figure 2 exhibits representative transmission electron microscopy (TEM) micrographs of the acid-treated samples that were created with TEOS flow rates of 5.0 and 2.5, respectively. The sample formed with the highest silica precursor flow rate studied [sample A, Fig. 2(a)] consists of nickel nanoparticles embedded in large clumps of amorphous silica. The powder formed under intermediate flow conditions [sample B, Fig. 2(b)] reveals evidence of similar nickel/silica structures, but

TABLE I. Mass percentage of each nickel/silica powder that survived treatment in hydrochloric acid.

| Sample name | TEOS flow rate (sccm) | Mass survival rate (%) | Average (%) |
|---------------|-----------------------|------------------------|-------------|
| A | 5 | 80.2 | 80.2 |
| B | 2.5 | 81.2 | 80.9 |
| B (replicate) | | 80.7 | |
| C | 1.5 | 31.3 | 30.2 |
| C (replicate) | | 29.0 | |
| D | 0.5 | 26.0 | 26.6 |
| D (replicate) | | 27.1 | |

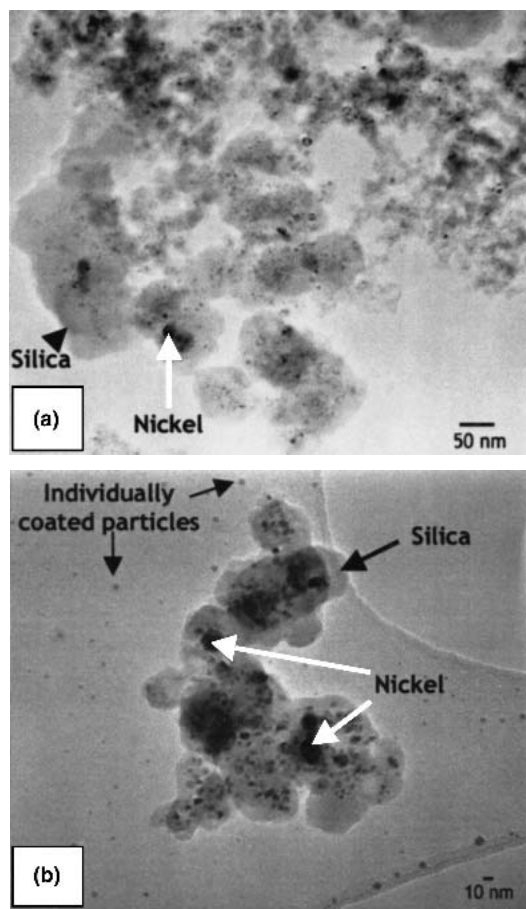


FIG. 2. TEM micrographs of nickel/silica powders following acid treatment: (a) sample A, consisting of protected nickel in large silica clumps; (b) sample B, containing similar clumps accompanied by individually coated particles.

those clusters are accompanied by a large number of individual particles that are well dispersed on the amorphous carbon film of the TEM grid. A histogram of the nickel particle size distribution from this sample (individually coated and embedded) is evident in Fig. 3. Note that the average particle size was calculated to be 6.2 nm, but a significant “tail” exists in the distribution at larger diameters. As discussed in Sec. III. C, the presence of these larger particles has an impact on the magnetic properties of the overall sample.

A higher magnification bright-field TEM image of the individual sample B particles and an x-ray diffraction pattern taken from the overall acid-treated sample are revealed in Fig. 4. A core/shell morphology is clearly depicted in the micrograph, and the spectrum verifies that face-centered-cubic nickel is the only crystalline species in the powder. Similar isolated particles were observed throughout the entire sample.

Lower levels of TEOS attempted during initial process experimentation (samples C and D of Table I) resulted in incomplete coverage of the nickel particles. Subsequent acid treatment and centrifugation of those powders yielded agglomerated empty shells (not shown). Energy dispersive x-ray and electron diffraction investigations of a large population of those shells (Fig. 5) confirmed that the coatings formed in this work are composed of amorphous silica.

On the basis of these results, a TEOS flow rate processing window has been identified for the production of individually separable nickel nanoparticles coated in silica. Below this flow rate, silica coverage is incomplete and the nickel particles are susceptible to dissolution in acid. Higher TEOS flow rates simply result in an excess of silica in the product, which serves to bind the individual nanoparticles together.

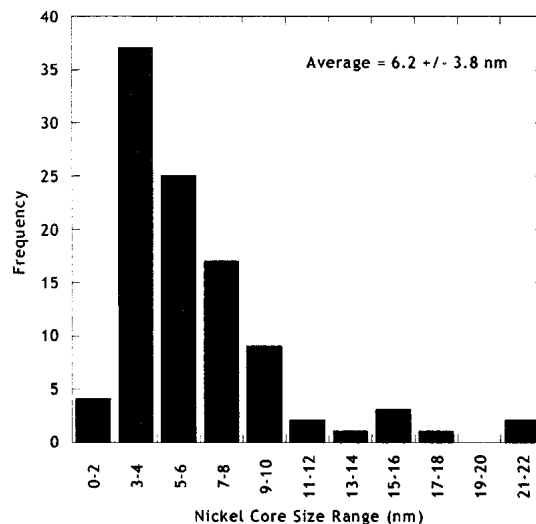


FIG. 3. Combined histogram of individually coated and bundled nickel particles from sample B.

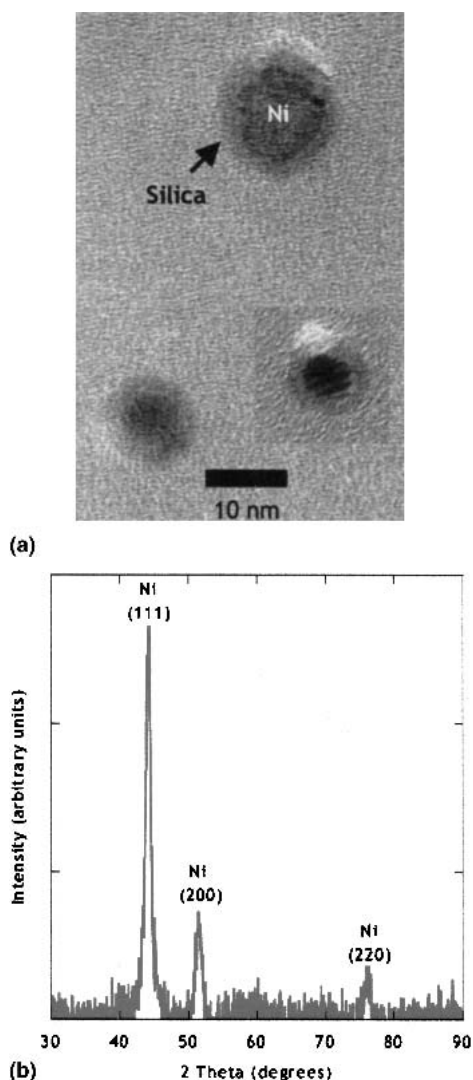


FIG. 4. (a) TEM micrographs of individual nickel/silica core/shell particles. (b) X-ray diffraction spectrum from acid-treated bulk sample B powder.

C. Magnetic measurements

Figure 6 displays the results of magnetic measurements taken from the acid-treated sample B. A peak in the zero-field-cooled plot, which is indicative of a superparamagnetic blocking temperature (T_B), can be seen at 41 K. However, this peak is not exceptionally well defined, and a gradual slope exists in the magnetization plot with increasing temperature. These features, as well as the presence of a small hysteresis (<100 Oe) at room temperature, reflect the shape variations and relatively broad particle size distribution evident in Figs. 2 and 3, respectively. Such characteristics are often associated with nanoparticles formed via an inert-gas blown-arc method and are likely the result of individual spherical particles agglomerating or sintering to different degrees prior to encapsulation by the silica.

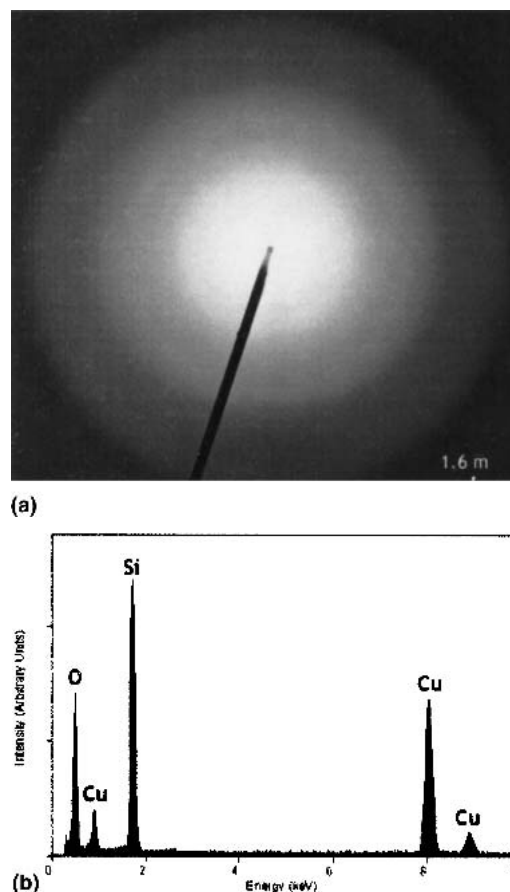


FIG. 5. (a) Electron diffraction pattern and (b) energy dispersive x-ray spectrum from empty shells formed during initial synthesis trials, confirming the chemistry and amorphous nature of the particle coatings. (The copper signal is from the TEM grid used to support the particles.)

Process modifications, such as increased helium quench jet velocity, have been shown to reduce the size and size distribution of magnetic particles in related work and may be pursued as a means to limit the occurrence of larger particles that yield a small hysteresis in the overall sample even at temperatures above the measured T_B . It is, nevertheless, quite encouraging to have synthesized SiO_x -coated magnetic nanoparticles exhibiting a superparamagnetic transition below room temperature, thereby allowing a colloidal suspension without significant magnetically induced agglomeration.

IV. SUMMARY

A hybrid processing method that combines magnetic nanoparticle synthesis via arc evaporation with subsequent coating formation by TEOS decomposition has been developed for the production of silica-coated magnetic nanoparticles. This synthesis approach offers an alternative to chemically prepared particles that may be subject to impurities. The amorphous silica coating affords protection to the metallic nanoparticles, shielding

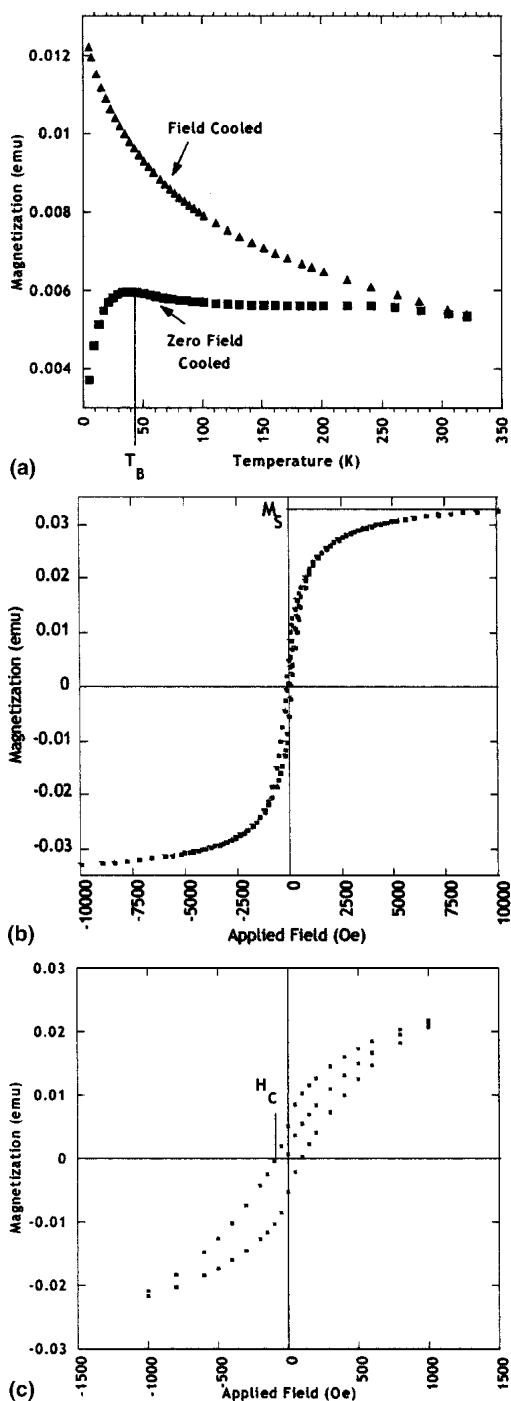


FIG. 6. (a) Field-cooled and zero-field-cooled plots of acid-treated sample B powder. The peak in the zero-field-cooled data indicates a superparamagnetic transition temperature (T_B) of approximately 41 K. (b) Magnetization versus applied field plot for the same powder. (c) An enlargement of (b) about the origin, displaying a small hysteresis ($H_c < 100$ Oe) at room temperature.

them from oxidation or dissolution in strong acids, and offers a surface for subsequent functionalization. Depending on the flow rate of the silica precursor, the morphology of well-protected samples may consist of

particles embedded in large silica clumps or individual (nickel core)/(silica shell) particles. Magnetic measurements conducted on a sample containing both types of coated particles revealed a superparamagnetic transition temperature of 41 K and a small hysteresis at room temperature. The latter is due to the presence of a small percentage of larger and irregularly shaped particles inherent in powders generated by inert gas blown-arc techniques. The processing method described in this paper offers the possibility that other magnetic materials may be coated in a similar manner.

ACKNOWLEDGMENTS

This work was supported by the Environmental Molecular Science Institute (EMSI) program of the National Science Foundation and the Department of Energy (Grant CHE-9810378) at the Northwestern University Institute for Environmental Catalysis. Additional financial support was supplied in the form of an Air Force Office of Scientific Research-Multidisciplinary University Research Initiative (AFOSR-MURI) grant.

REFERENCES

1. M. Meza, in *Scientific and Clinical Applications of Magnetic Carriers*, edited by U. Hafeli, W. Schutt, J. Teller, and M. Zborowski (Plenum Press, New York, 1997), pp. 303–309.
2. J.W.M. Bulte and R.A. Brooks, in *Scientific and Clinical Applications of Magnetic Carriers*, edited by U. Hafeli, W. Schutt, J. Teller, and M. Zborowski (Plenum Press, New York, 1997), pp. 527–543.
3. A. Jordan, P. Wust, R. Scholz, H. Faehling, J. Krause, and R. Felix, in *Scientific and Clinical Applications of Magnetic Carriers*, edited by U. Hafeli, W. Schutt, J. Teller, and M. Zborowski (Plenum Press, New York, 1997), pp. 569–595.
4. P.F. Renshaw, C.S. Owen, A.C. McLaughlin, T.G. Frey, and J.J.S. Leigh, *Magn. Reson. Med.* **3**, 217 (1986).
5. R.E. Rosenweig, *Chem. Eng. Prog.* **85**, 53 (1989).
6. S. Onodera, H. Kondo, and T. Kawana, *MRS Bull.* **21**(9), 35 (1996).
7. K. O'Grady, R.L. White, and P.J. Grundy, *J. Magn. Mater.* **177–181**, 886 (1998).
8. R.L. White, R.M.H. New, and R.F.W. Pease, *IEEE Trans. Magn.* **33**, 990 (1997).
9. S. Seraphin, D. Zhou, J. Jiao, J.C. Withers, and R. Loutfy, *Appl. Phys. Lett.* **63**, 2073 (1993).
10. S. Bandow and Y. Saito, *Jpn. J. Appl. Phys.* **32**, L1677 (1993).
11. Y. Saito, T. Yoshikawa, M. Okuda, N. Fujimoto, K. Sumiyama, K. Suzuki, A. Kasuya, and Y. Nishina, *J. Phys. Chem. Solids* **54**, 1849 (1993).
12. Y. Saito, M. Okuda, T. Yoshikawa, A. Kasuya, and Y. Nishina, *J. Phys. Chem.* **98**, 6696 (1994).
13. S.A. Majetich, J.O. Artman, M.E. McHenry, N.T. Nuhfer, and S.W. Staley, *Phys. Rev. B: Condens. Matter.* **48**, 16845 (1993).
14. Y. Saito, *Carbon* **33**, 979 (1995).
15. S. Seraphin, *J. Electrochem. Soc.* **142**, 290 (1995).
16. V.P. Dravid, M-H. Teng, J.J. Host, B.R. Elliott, D.L. Johnson, T.O. Mason, J.R. Weertman, and J-H. Hwang, United States Patent No. 5 472 749 (5 December 1995).

17. V.P. Dravid, J.J. Host, M.H. Teng, B. Elliott, J. Hwang, D.L. Johnson, T.O. Mason, and J.R. Weertman, *Nature* **374**, 602 (1995).
18. J.J. Host, M.H. Teng, B.R. Elliott, J-H. Hwang, T.O. Mason, D.L. Johnson, and V.P. Dravid, *J. Mater. Res.* **12**, 1268 (1997).
19. K.L. Klug, Ph.D. Dissertation, Northwestern University (2002).
20. G. Ennas, A. Mei, A. Musinu, G. Piccaluga, G. Pinna, and S. Solinas, *J. Non-Cryst. Solids* **232–234**, 587 (1998).
21. G. Wang and A. Harrison, *J. Colloid Interface Sci.* **217**, 203 (1999).
22. M. Ohmori and E. Matijevic, *J. Colloid Interface Sci.* **160**, 288 (1993).
23. S. Hui, Y.D. Zhang, T.D. Xiao, M. Wu, S. Ge, W.A. Hines, J.I. Budnick, M.J. Yacaman, and H.E. Troiani, in *Nanophase and Nanocomposite Materials IV*, edited by S. Komarneni, R.A. Vaia, G.Q. Lu, J-I. Matsushita, and J.C. Parker (Mater. Res. Soc. Symp. Proc. **703**, Warrendale, PA, 2002).
24. A.P. Philipse, M.P.B.v. Bruggen, and C. Pathmamanoharan, *Langmuir* **10**, 92 (1994).
25. M.R. Zachariah, R.D. Shull, B.K. McMillin, and P. Biswas, in *Nanotechnology Molecularly Designed Materials*, edited by G-M. Chow and K.E. Gonsalves (American Chemical Society, Washington, DC, 1996), p. 42.
26. Q. Liu, Z. Xu, J.A. Finch, and R. Egerton, *Chem. Mater.* **10**, 3936 (1998).
27. S. Hui, Y.D. Zhang, T.D. Xiao, M. Wu, S. Ge, W.A. Hines, J.I. Budnick, M.J. Yacaman, and H.E. Troiani, in *Nanophase and Nanocomposite Materials IV*, edited by S. Komarneni, R.A. Vaia, G.Q. Lu, J-I. Matsushita, and J.C. Parker (Mater. Res. Soc. Symp. Proc. **703**, Warrendale, PA, 2002).
28. L.M. Liz-Marzan, M. Giersig, and P. Mulvaney, *Langmuir* **12**, 4329 (1996).
29. C. Radloff and N.J. Halas, *Appl. Phys. Lett.* **79**, 674 (2001).
30. T. Ung, L.M. Liz-Marazan, and P. Mulvaney, *Langmuir* **14**, 3740 (1998).
31. T. Li, J. Moon, A.A. Morrone, J.J. Mecholsky, D.R. Talham, and J.H. Adair, *Langmuir* **15**, 4328 (1999).
32. C-S. Yang, S.M. Kauzlarich, and Y.C. Wang, *Chem. Mater.* **11**, 3666 (1999).
33. A.N. Patil, R.P. Andres, and N. Otsuka, *J. Phys. Chem.* **98**, 9247 (1994).
34. W-H. Shih, D. Kisailus, and Y. Wei, *Mater. Lett.* **24**, 13 (1995).
35. C. Beck, W. Hartl, and R. Hempelmann, *Angew. Chem., Int. Ed.* **38**, 1297 (1999).
36. E. Bourgeat-Lami, P. Espiard, and A. Guyot, *Polymer* **36**, 4385 (1995).
37. G. Deng, M.A. Markowitz, P.R. Kust, and B.P. Gaber, *Mater. Sci. Eng. C* **11**, 165 (2000).
38. J.W. Goodwin, R.S. Harbron, and P.A. Reynolds, *Colloid Polym. Sci.* **268**, 766 (1990).
39. M. Qhobosheane, S. Santra, P. Zhang, and W. Tan, *Analyst* **126**, 1274 (2001).
40. S. Spange and A. Reuter, *Langmuir* **15**, 141 (1999).
41. S. Spange, *Prog. Polym. Sci.* **25**, 781 (2000).
42. B. Vincent, *Chem. Eng. Sci.* **48**, 429 (1993).
43. S.L. Westcott, S.J. Oldenburg, T.R. Lee, and N.J. Halas, *Langmuir* **14**, 5396 (1998).
44. C. Graf and A.v. Blaaderen, *Langmuir* **18**, 524 (2002).
45. B. Saoudi, N. Jammul, M.M. Chehimi, G.P. McCarthy, and S.P. Armes, *J. Colloid Interface Sci.* **192**, 269 (1997).
46. I. Voigt, F. Simon, K. Esthel, S. Spange, and M. Friedrich, *Langmuir* **17**, 8355 (2001).
47. K.L. Klug, D.L. Johnson, and V.P. Dravid, in *Advanced Hard and Soft Magnetic Materials*, edited by L.H.L.M. Coey, B-M. Ma, T. Schrefl, L. Schultz, J. Fidler, V.G. Harris, R. Hasegawa, A. Inoue, and M. McHenry (Mater. Res. Soc. Symp. Proc. **577**, Warrendale, PA, 1999), pp. 405–408.